Inorganic Chemistry
Article

Inorg. Chem. **2009**, *48*, 9631–9643 **9631**
DOI: 10.1021/ic900653q

On the Viability of Cyclometalated Ru(II) Complexes for Light-Harvesting Applications

Paolo G. Bomben, Kiyoshi C. D. Robson, Pavel A. Sedach, and Curtis P. Berlinguette*

Department of Chemistry and The Institute of Sustainable Energy, Environment and Economy, University of Calgary, 2500 University Drive N.W., Calgary, Canada T2N-1N4

Received April 3, 2009

The effects of replacing a single polypyridyl ligand with an analogous anionic cyclometalating ligand were investigated for a set of three structurally related series of Ru(II) compounds formulated as $[Ru(bpy)_2(L)]^z$, $[Ru(tpy)(L)]^z$, and $[Ru(tpy)(L)Cl]^z$, where $z = 0$, $+1$, or $+2$, and L = polypyridyl (e.g., bpy = 2,2′-bipyridine, tpy = 2,2′:6′,2″-terpyridine) or cyclometalating ligand (e.g., deprotonated forms of 2-phenylpyridine or 3−(2−pyridinyl)-benzoic acid). Each of the complexes were synthesized and characterized by ^{1}H NMR spectroscopy, electrospray ionization mass spectrometry (ESI-MS), and/or elemental analyses (EA). Cyclic voltammetry reveals that cyclometalation causes a shift of the first oxidation and reduction potentials by −0.5 to −0.8 V and −0.2 to −0.4 V, respectively, relative to their polypyridyl congeners. These disparate shifts have the effect of inducing a bathochromic shift of the lowest-energy absorption bands by as much as 90 nm. With the aid of time-dependent density functional theory (DFT), the lowest-energy bands (λ_{max} = 500−575 nm) were assigned as predominantly metal-to-ligand charge-transfer (MLCT) transitions from Ru to the polypyridyl ligands, while Ru→*C^N* (or *C^N^N* or *N^C^N*) transitions are found within the absorption bands centered at ca. 400 nm. The properties of a series of compounds furnished with carboxylic acid anchoring groups at various positions are also examined for applications involving the sensitization of metal-oxide semiconductors. It is determined that the thermodynamic potentials of many of these compounds are appropriate for conventional photoelectrochemical cells (e.g., dye-sensitized solar cells) that utilize a titania electrode and iodide-based electrolyte.

Introduction

While a host of architectures and materials are being pursued to replace (multi)crystalline-Si and other thin-film technologies, the dye-sensitized solar cell (DSSC) developed by Grätzel continues to stand out as the most efficient "next-generation" technology with certified power conversion efficiencies (η) in excess of 10%.[1,2] The photosensitizer represents a critical component for achieving high power conversion efficiencies in the DSSC. The ideal dye should absorb as much visible light as possible, have redox potentials appropriately matched to the semiconductor and electrolyte for electron-injection and regeneration, respectively, and sustain numerous redox turnovers under light irradiation.[3] Satisfying these requirements has proven to be extremely difficult: to date, only a limited set of Ru-polypyridyl complexes have been documented to produce $\eta > 10\%$.[4,5]

The mechanism of sensitization within a prototypical Ru-based dye, such as $[Ru(dcbpy)_2(NCS)_2]$ (**N3**; dcbpy = 2,2′-dipyridyl-4,4′-dicarboxylic acid; Figure 1a), relies on a light-driven metal-to-ligand charge-transfer (MLCT) transition that facilitates rapid charge-injection into the semiconductor anode.[5−7] To harness a greater fraction of the solar spectrum, most research in the realm of Ru-based chromophores is targeted at driving the MLCT band to longer wavelengths.[4] The typical procedure is to either lower the π^* manifold of the polypyridyl ligand or raise the energy of the metal-based highest occupied molecular orbital (HOMO) using strong donor ligands (e.g., NCS^-).[8] Recent efforts have focused on using long conjugated substituents as a means of lowering the π^* orbital to capture lower-energy photons, with the added benefit of impeding back electron-transfer between the anode and the electrolyte (e.g., I^-/I^-_3).[9]

Departing from this methodology, our program has set out to explore the viability of using cyclometalated (*C^N*) Ru complexes in the DSSC setting. This approach follows the work of Thompson et al., who measured the performance of a cyclometalated Ir complex, $[Ir(ppz)_2(dcbpy)]^+$

*To whom correspondence should be addressed. E-mail: cberling@ucalgary.ca.

(1) O'Regan, B.; Grätzel, M. *Nature* **1991**, *353*, 737–740.
(2) Green, M. A.; Emery, K.; Hishikawa, Y.; Warta, W. *Prog. Photovoltaics* **2009**, *17*, 85–94.
(3) Grätzel, M. *Nature* **2001**, *414*, 338–344.
(4) Robertson, N. *Angew. Chem., Int. Ed.* **2008**, *47*, 1012–1014.
(5) Ardo, S.; Meyer, G. J. *Chem. Soc. Rev.* **2009**, *38*, 115–164.
(6) Juris, A.; Balzani, V.; Barigelletti, F.; Campagna, S.; Belser, P.; Von Zelewsky, A. *Coord. Chem. Rev.* **1988**, *84*, 85–277.
(7) Sauvage, J. P.; Collin, J. P.; Chambron, J. C.; Guillerez, S.; Coudret, C.; Balzani, V.; Barigelletti, F.; De Cola, L.; Flamigni, L. *Chem. Rev.* **1994**, *94*, 993–1020.
(8) Grätzel, M. *Inorg. Chem.* **2005**, *44*, 6841–6851.
(9) Wang, P.; Klein, C.; Humphry-Baker, R.; Zakeeruddin, S. M.; Grätzel, M. *J. Am. Chem. Soc.* **2005**, *127*, 808–809.

Published on Web 09/23/2009

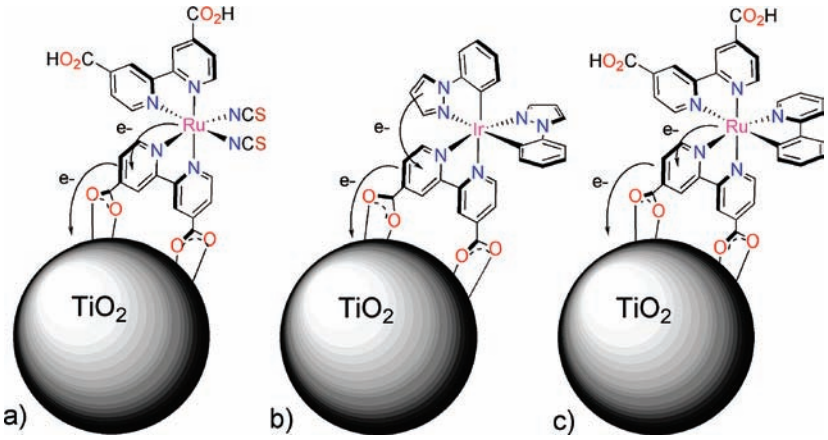

Figure 1. Sensitization modes for the inorganic dyes (a) [Ru(dcbpy)(NCS)$_2$] (**N3**; MLCT),[5−7] (b) [Ir(ppz)$_2$(dcbpy)]$^+$ (LLCT),[10] and (c) [Ru(dcbpy)$_2$(ppy)]$^+$ (MLCT) anchored to TiO_2.

(ppz = phenylpyrazolyl), in the DSSC.[10] While their efforts were rewarded with a positive photovoltaic response, the mode of sensitization operative within this complex is based on a ppz→dcbpy ligand-to-ligand charge-transfer (LLCT) process (Figure 1b), By utilizing a similar coordination environment about a Ru center, we reasoned that this LLCT process could be bypassed in favor of a lower-energy MLCT transition (Figure 1c). We and others[11] have advanced this concept on the basis that this coordination environment should shift the absorbance profile closer to the near-infrared (NIR) region of the spectrum, and that the M−C σ-bonding arrangement could yield a more robust chromophore in the DSSC setting.

Our initial foray into this area involves the examination of the electrochemical and photophysical properties of $C^\wedge N$ analogues of bipyridine and phenanthroline, as well as the $C^\wedge N^\wedge N$ and $N^\wedge C^\wedge N$ analogues of terpyridine coordinated to a Ru(II) center. Building on the pioneering work of Constable[12−16] and Selbin,[17] the syntheses of many complexes of this type have been previously reported.[18−29] The utility of these complexes in the DSSC, however, had not been documented until a recent study by van Koten and co-workers.[11] While the performance of a set of [Ru(tpy)($C^\wedge N^\wedge N$)]$^+$ complexes in the DSSC was shown to be modest compared to champion Ru-based dyes, their study demonstrated a new paradigm of chromophore design. This strategy has been corroborated by Grätzel et al., who recently documented power conversion efficiencies in excess of 10% using the cyclometalated complex, [Ru(dcbpy)(ppy-F$_2$)]$^+$ (ppy-F$_2$ = 2-(2,4-difluorophenyl)pyridine).[30]

Expanding on these studies, we have set out to unravel the underlying mode of sensitization in a related family of bidentate and tridentate complexes (Figure 2). Included in this analysis are three independent series of compounds denoted as [Ru(bpy)$_2$(L)]^z, [Ru(tpy)(L)]^z, and [Ru(tpy)(L)Cl]^z (z = 0, +1, or +2; L = polypyridyl ligand or cyclometalating ligand); the latter series represents a *neutral* set of cyclometalated compounds that have limited precedent in the literature.[31] We note that the properties of a related series of Ru($C^\wedge N^\wedge N$) and Ru($N^\wedge C^\wedge N$) complexes were recently catalogued by van Koten et al.[32] Results from our study verify that the lowest-energy transitions for these complexes are dominated by mixed metal-ligand to ligand charge-transfer excitation processes. The lowest unoccupied molecular orbital (LUMO) and HOMO levels for the [Ru(bpy)$_2$(L)]^z and [Ru(tpy)(L)]^z series are appropriately positioned relative

(10) Mayo, E. I.; Kilsa, K.; Tirrell, T.; Djurovich, P. I.; Tamayo, A.; Thompson, M. E.; Lewis, N. S.; Gray, H. B. *Photochem. Photobiol. Sci.* **2006**, *5*, 871–873.
(11) Wadman, S. H.; Kroon, J. M.; Bakker, K.; Lutz, M.; Spek, A. L.; van Klink, G. P. M.; van Koten, G. *Chem. Commun* **2007**, 1907–1909.
(12) Constable, E. C.; Hannon, M. J. *Inorg. Chim. Acta* **1993**, *211*, 101–110.
(13) Constable, E. C.; Thompson, A. M. W. C.; Tocher, D. A.; Daniels, M. A. M. *New J. Chem.* **1992**, *16*, 855–867.
(14) Constable, E. C.; Housecroft, C. E. *Polyhedron* **1990**, *9*, 1939–1947.
(15) Constable, E. C.; Leese, T. A. *J. Organomet. Chem.* **1987**, *335*, 293–299.
(16) Constable, E. C.; Holmes, J. M. *J. Organomet. Chem.* **1986**, *301*, 203–208.
(17) Reveco, P.; Cherry, W. R.; Medley, J.; Garber, A.; Gale, R. J.; Selbin, J. *Inorg. Chem.* **1986**, *25*, 1842–1845.
(18) Barigelletti, F.; Ventura, B.; Collin, J.-P.; Kayhanian, R.; Gavina, P.; Sauvage, J.-P. *Eur. J. Inorg. Chem.* **2000**, 113–119.
(19) Patoux, C.; Launay, J.-P.; Beley, M.; Chodorowski-Kimmes, S.; Collin, J.-P.; James, S.; Sauvage, J.-P. *J. Am. Chem. Soc.* **1998**, *120*, 3717–3725.
(20) Collin, J.-P.; Kayhanian, R.; Sauvage, J.-P.; Calogero, G.; Barigelletti, F.; De Cian, A.; Fischer, J. *Chem. Commun.* **1997**, 775–776.
(21) Collin, J. P.; Beley, M.; Sauvage, J. P.; Barigelletti, F. *Inorg. Chim. Acta* **1991**, *186*, 91–93.
(22) Ott, S.; Borgström, M.; Hammarström, L.; Johansson, O. *Dalton Trans.* **2006**, 1434–1443.
(23) Le Lagadec, R.; Rubio, L.; Alexandrova, L.; Toscano, R. A.; Ivanova, E. V.; Meskys, R.; Laurinavicius, V.; Pfeffer, M.; Ryabov, A. D. *J. Organomet. Chem.* **2004**, *689*, 4820–4832.
(24) Sortais, J.-B.; Pannetier, N.; Holuigue, A.; Barloy, L.; Sirlin, C.; Pfeffer, M.; Kyritsakas, N. *Organometallics* **2007**, *26*, 1856–1867.
(25) Leyva, L.; Sirlin, C.; Rubio, L.; Franco, C.; Le Lagadec, R.; Spencer, J.; Bischoff, P.; Gaiddon, C.; Loeffler, J. P.; Pfeffer, M. *Eur. J. Inorg. Chem.* **2007**, *2007*, 3055–3066.
(26) Saavedra-Diaz, O.; Ceron-Camacho, R.; Hernandez, S.; Ryabov, A. D.; Le Lagadec, R. *Eur. J. Inorg. Chem.* **2008**, 4866–4869.
(27) Ryabov, A. D.; Estevez, H.; Alexandrova, L.; Pfeffer, M.; Le Lagadec, R. *Inorg. Chim. Acta* **2006**, *359*, 883–887.
(28) Le Lagadec, R.; Alexandrova, L.; Estevez, H.; Pfeffer, M.; Laurinavicius, V.; Razumiene, J.; Ryabov, A. D. *Eur. J. Inorg. Chem.* **2006**, *2006*, 2735–2738.
(29) Alpeeva, I. S.; Soukharev, V. S.; Alexandrova, L.; Shilova, N. V.; Bovin, N. V.; Csoeregi, E.; Ryabov, A. D.; Sakharov, I. Y. *J. Biol. Inorg. Chem.* **2003**, *8*, 683–688.
(30) Bessho, T.; Yoneda, E.; Yum, J.-H.; Guglielmi, M.; Tavernelli, I.; Imai, H.; Rothlisberger, U.; Nazeeruddin, M. K.; Grätzel, M. *J. Am. Chem. Soc.* **2009**, *131*, 5930–5934.
(31) Li, E. Y.; Cheng, Y.-M.; Hsu, C.-C.; Chou, P.-T.; Lee, G.-H.; Lin, I. H.; Chi, Y.; Liu, C.-S. *Inorg. Chem.* **2006**, *45*, 8041–8051.
(32) Wadman, S. H.; Lutz, M.; Tooke, D. M.; Spek, A. L.; Hartl, F.; Havenith, R. W. A.; van Klink, G. P. M.; van Koten, G. *Inorg. Chem.* **2009**, *48*, 1887–1900.

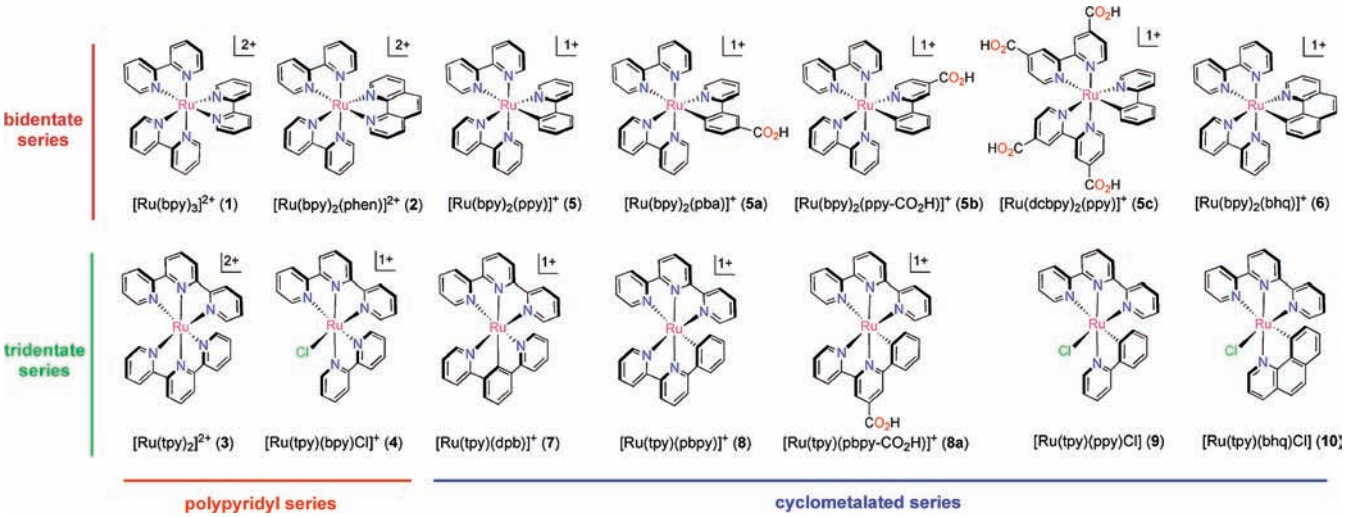

Figure 2. Polypyridyl and Cyclometalated Ru(II) Complexes Under Investigation. "Polypyridyl" denotes that the complex lacks a cyclometalating ligand; "tridentate" denotes that the complex contains a tpy ligand. Counterion = PF_6^- for all complexes except **5b**, which is isolated as the NO_3^- salt; bpy = 2,2′-bipyridine; phen = 1,10-phenanthroline; tpy = 2,2′:6′,2″-terpyridine; Hppy = 2-phenylpyridine; Hpba = 3-(2-pyridinyl)-benzoic acid; Hppy-CO_2H = 2-phenylpyridine-4-carboxylic acid; Hbhq = benzo[*h*]quinoline; dcbpy = 2,2'-dipyridyl-4,4'-dicarboxylic acid; Hpbpy = 6-phenyl-2,2'−bipyridine; Hpbpy−CO_2H = 6-phenyl-[2,2'-bipyridine]-4-carboxylic acid; Hdpb = 1,3-bis(2-pyridyl)benzene.

to the TiO_2 conducting band and redox potential of the electrolyte (i.e., I^-/I_3^-) found in the standard DSSC framework. We also assess the best strategy for positioning the —CO_2H anchoring groups about the bidentate molecules for optimal sensitization. The work presented herein underscores the potential utility of this class of chromophores in the DSSC setting.

Experimental Section

Preparation of Compounds. All manipulations were performed using solvents passed through an MBraun solvent purification system prior to use; chloroform ($CHCl_3$) and tetrahydrofuran (THF) solvents were analytical grade (without stabilizer). All reagents were purchased from Aldrich, except for $RuCl_3$ (Pressure Chemical Company), bpy and dcbpy (Alfa Aesar), and Hpba (Synchem). Purification by column chromatography was carried out using silica (Silicycle: Ultrapure Flash Silica) or basic alumina (Fluka). Analytical thin-layer chromatography (TLC) was performed on aluminum-backed sheets pre-coated with silica 60 F254 adsorbent (0.25 mm thick; Merck, Germany), or with plastic-backed sheets pre-coated with basic alumina 200 F254 adsorbent (0.25 mm thick, Selecto Scientific: Georgia, U.S.A.) and visualized under UV light. Ligands Hdpb,[33] Hpbpy,[34] Hpbpy−CO_2H,[32] [Ru(ppy)(MeCN)$_4$](PF_6)[35] and compounds **1**,[36] **2**,[37] **3**,[38] **4**,[39] **5**,[16] **6**,[17] **7**,[38] and **8**[40] were prepared according to published procedures (with additional purification by column chromotagraphy).

2-Bromopyridine-4-carboxylic Acid. To 1.84 g (11.6 mmol) of $KMnO_4$ in 10 mL of H_2O was added 0.65 mL (5.8 mmol) of 2-bromo-4-methylpyridine via syringe. The solution was refluxed for 1 h, after which 1.25 equiv (1.15 g; 7.25 mmol) of $KMnO_4$ was added. After an additional 2 h reflux, 1.25 equiv of $KMnO_4$ was added and stirred overnight to produce a dark solution containing a black suspension. After filtration through Celite, the clear aqueous layer was washed with 3 × 20 mL of ethyl acetate. The aqueous layer was brought to a pH of 4 using 1 M HCl to precipitate out 239 mg of a white solid (yield = 20.3%). ESI-MS: *m*/*z* 199.7 (calcd for M^+ 199.9) ^{1}H NMR (DMSO-d_6): δ 7.84 (dd, 1H, ^3J = 5 Hz, ^4J = 1 Hz), 7.96 (s, 1H), 8.59 (d, 1H, ^3J = 5 Hz), 14.02 (vbr, 1H).

2-Phenylpyridine-4-carboxylic Acid (Hppy-CO_2H). To a flask containing 239 mg (1.18 mmol) of 2-bromopyridine-4-carboxylic acid, 213 mg (1.75 mmol) of phenylboronic acid, and 26 mg (0.12 mmol) of $Pd(OAc)_2$ was added a large excess of K_2CO_3 (1627 mg, 11.79 mmol) in 20 mL of H_2O. The solution was refluxed overnight to produce a dark black suspension that was filtered to yield a dark black filtrate, which was then acidified to a pH of 4 using 2 M HCl to precipitate 110 mg of a white solid (yield = 47%). ^{1}H NMR (DMSO-d_6): δ 7.50 (m, 3H), 7.77 (dd, 1H, ^3J = 5 Hz, ^4J = 1 Hz), 8.12 (d, 2H, ^3J = 5 Hz), 8.28 (s, 1H), 8.85 (d, 1H, ^3J = 5 Hz), 13.85 (vbr, 1H)

1,3-Bis(2-pyridyl)benzene (Hdpb). An alternative synthesis to the one previously reported is provided.[33] A THF (150 mL) solution containing 1.95 g (8.30 mmol) of 1,3-dibromobenzene and 0.077 g (0.66 mol) of *tetrakis*(triphenylphosphine)palladium(0) was charged with 38 mL (17 mmol) of a 0.5 M THF solution of 2-pyridylzinc bromide. The solution was refluxed for 14 h, then cooled and quenched with a saturated aqueous $NaHCO_3$ solution (100 mL) and washed with aqueous EDTA (100 mL). The crude product was extracted with diethyl ether (2 × 100 mL), and the organic fractions were collected and dried over $MgSO_4$. The solvent was removed in vacuo to afford an oil that was purified by column chromatography (silica; EtOAc:DCM 1:9) to afford 1.8 g of a pale yellow oil product (yield = 94%). GC-MS: *m*/*z* 232. ^{1}H NMR ($CDCl_3$): δ 7.06 (t, 2H, ^3J = 6 Hz), 7.46 (t, 1H, ^3J = 8 Hz), 7.57 (t, 2H, ^3J = 7 Hz), 7.68 (d, 2H, ^3J = 8 Hz), 7.96 (d, 2H, ^3J = 8 Hz), 8.59 (s, 1H), 8.60 (d, 2H, ^3J = 7 Hz).

6-Phenyl-2,2′-bipyridine (Hpbpy). An alternative synthesis to one reported previously is provided.[34] A solution of phenyl lithium (3.60 mL, 6.48 mmol) was injected into 20 mL of toluene containing 1.00 g (6.43 mmol) of bpy. The red solution was refluxed overnight to produce a purple solution that was cooled to room temperature, and then transferred into a separatory

(33) Soro, B.; Stoccoro, S.; Minghetti, G.; Zucca, A.; Cinellu, M. A.; Gladiali, S.; Manassero, M.; Sansoni, M. *Organometallics* **2005**, *24*, 53–61.
(34) Hebbe-Viton, V.; Desvergnes, V.; Jodry, J. J.; Dietrich-Buchecker, C.; Sauvage, J.-P.; Lacour, J. *Dalton Trans.* **2006**, 2058–2065.
(35) Fernandez, S.; Pfeffer, M.; Ritleng, V.; Sirlin, C. *Organometallics* **1999**, *18*, 2390–2394.
(36) Broomhead, J. A.; Young, C. G. *Inorg. Synth.* **1981**, 127.
(37) Huang, W.; Ogawa, T. *Polyhedron* **2006**, *25*, 1379–1385.
(38) Schubert, U. S.; Eschbaumer, C.; Andres, P.; Hofmeier, H.; Weidl, C. H.; Herdtweck, E.; Dulkeith, E.; Morteani, A.; Hecker, N. E.; Feldmann, J. *Synth. Met.* **2001**, *121*, 1249–1252.
(39) Yang, X.-J.; Drepper, F.; Wu, B.; Sun, W.-H.; Haehnel, W.; Janiak, C. *Dalton Trans.* **2005**, 256–267.
(40) Barigelletti, F.; Flamigni, L.; Balzani, V.; Collin, J. P.; Sauvage, J. P.; Sour, A.; Constable, E. C.; Thompson, A. M. W. C. *J. Chem. Soc., Chem. Commun.* **1993**, 942–944.

funnel and washed with 30 mL of water. The aqueous layer was washed with dichloromethane (3 × 15 mL), and the organic layers were pooled and dried with $MgSO_4$. After filtration, the solvent was removed in vacuo to yield a red oil, and then purified by column chromatography (silica; Et_2O/hexanes 3:7). The solvent was removed in vacuo to yield 562 mg of an off-white crystalline product (yield = 37.7%). GC-MS: m/z 232 (calcd for $\{M\}^+$ 232). ^{1}H NMR ($CDCl_3$): δ 7.30 (ddd, 1H, ^3J = 8 Hz, ^3J = 8 Hz, ^4J = 1 Hz), 7.42 (dt, 1H, ^3J = 7 Hz, ^4J = 1 Hz), 7.49 (tt, 2H, ^3J = 7 Hz, ^4J = 1 Hz), 7.76 (dd, 1H, ^3J = 8 Hz, ^4J = 1 Hz), 7.82 (dt, 1H, ^3J = 8 Hz, ^4J = 1 Hz), 7.88 (t, 1H, ^3J = 8 Hz), 8.13 (dt, 2H, ^3J = 8 Hz, ^4J = 1 Hz), 8.35 (dd, 1H, ^3J = 8 Hz, ^4J = 1 Hz), 8.62 (dt, 1H, ^3J = 8 Hz, ^4J = 1 Hz), 8.67 (ddd, 1H, ^3J = 5 Hz, ^3J = 5 Hz, ^4J = 1 Hz).

[Ru(bpy)$_2$(ppy)]PF$_6$(5). In accord with a previously described procedure,[16] a flask containing 196 mg (0.377 mmol) of Ru(bpy)$_2$Cl$_2$, 152 mg (0.784 mmol) of $AgBF_4$, and 0.16 mL (1.1 mmol) of 2-phenylpyridine in 30 mL of dichloromethane was stirred at reflux for 21 h. The solution was left to cool to room temperature, filtered through Celite to afford a dark red-purple filtrate and concentrated to 5 mL. After the addition of 200 mL of hexanes, the solution was left to stand at 4 °C overnight to afford a dark red-purple solid that was filtered and washed with water (3 × 15 mL). The solid was dissolved in acetonitrile to carry out anion metathesis using a saturated aqueous NH_4PF_6 solution to render a dark purple precipitate. This solid was collected and washed with water (3 × 15 mL) and diethyl ether (3 × 15 mL) to afford 150 mg of a purple solid (yield = 55.0%). ^{1}H NMR (CD_3CN): 6.41 (dd, 1H, ^3J = 7 Hz, ^4J = 1 Hz), 6.82 (dt, 1H, ^3J = 5 Hz, ^4J = 1 Hz), 6.89 (dt, 1H, ^3J = 5 Hz, ^4J = 1 Hz), 6.92 (ddd, 1H, ^3J = 7 Hz, 5 Hz, ^4J = 1 Hz), 7.20 (m, 3H), 7.40 (ddd, 1H, ^3J = 8 Hz, 5 Hz, ^4J = 1 Hz), 7.55 (ddd, 1H, ^3J = 5 Hz, ^4J = 2 Hz, ^5J = 1 Hz), 7.68 (ddd, 1H, ^3J = 8 Hz, 7 Hz, ^4J = 1 Hz), 7.72 (dd, 1H, ^3J = 5 Hz, ^4J = 1 Hz, ^5J = 1 Hz), 7.82 (m, 6H), 7.97 (ddd, 1H, ^3J = 8 Hz, 7 Hz, ^4J = 1 Hz), 8.01 (d, 1H, ^3J = 8 Hz), 8.05 (ddd, 1H, ^3J = 5 Hz, ^4J = 2 Hz, ^5J = 1 Hz), 8.29 (d, 1H, ^3J = 8 Hz), 8.31 (d, 1H, ^3J = 8 Hz), 8.35 (d, 1H, ^3J = 8 Hz), 8.45 (d, 1H, ^3J = 8 Hz). ESI-MS: m/z 568.0 (calcd for $\{M^+\}$ 568.1) HRMS (MALDI-TOF): m/z = 568.11050 [(M)+] (calcd for $C_{31}H_{24}N_5Ru^+$: m/z = 568.10779).

[Ru(bpy)$_2$(pba)]PF$_6$ (5a). To a flask containing 95 mg (0.48 mmol) of 3-(pyridin-2-yl)benzoic acid and 20 mg (0.50 mmol) of NaOH was added 30 mL of degassed aqueous methanol solution (H_2O/MeOH 1:5 v/v). The reagents were stirred until all components were dissolved and then transferred to a flask containing 188 mg (0.362 mmol) of Ru(bpy)$_2$Cl$_2$ and 180 mg (0.93 mmol) of $AgBF_4$. The reaction mixture was heated at reflux for 18 h, cooled, and then filtered through Celite to afford a dark red/purple filtrate. The solvent was removed in vacuo and then passed through a silica column (MeCN/$KNO_{3(aq)}$ 7:1 v/v), followed by anion exchange with a saturated aqueous NH_4PF_6 methanolic solution to produce 52 mg of a red precipitate (yield = 19%). ^{1}H NMR (CD_3CN): 6.61 (d, 1H, ^3J = 8 Hz), 6.98 (dt, 1H, ^3J = 7 Hz, 6 Hz, ^4J = 1 Hz), 7.17−7.25 (m, 3H), 7.39, (dd, 1H, ^3J = 8 Hz, ^4J = 2 Hz), 7.42 (dt, 1H, ^3J = 8 Hz, ^4J = 1 Hz), 7.60 (d, 1H, ^3J = 5 Hz), 7.69−7.75 (m, 3H), 7.78−7.87 (m, 4H), 7.95 (d, 1H, ^3J = 6 Hz), 7.99 (dt, 1H, ^3J = 8 Hz, ^4J = 2 Hz), 8.14 (d, 1H, ^3J = 8 Hz), 8.31 (d, 1H, ^3J = 7 Hz), 8.33 (d, 1H, ^3J = 7 Hz), 8.38 (d, 1H, ^3J = 8 Hz), 8.41 (d, 1H, ^4J = 2 Hz), 8.46 (d, 1H, ^3J = 8 Hz), 9.08 (vbr, 1H). ESI-MS: m/z 612.1 (calcd for $\{M^+\}$ 612.1) Anal. Calcd for $C_{32}H_{24}F_6N_5O_2PRu$ + 0.5 H_2O: C, 50.20; H, 3.29; N, 9.15. Found: C, 50.29; H, 3.49; N, 9.07.

[Ru(bpy)$_2$(ppy-CO$_2$H)]NO$_3$ (5b). To a flask containing 110 mg (0.553 mmol) of Hppy-CO_2H, 275 mg (0.529 mmol) of Ru(bpy)$_2$Cl$_2$, 183 mg (1.08 mmol) of $AgNO_3$, and 28 mg (0.70 mmol) of NaOH was added 30 mL of a degassed aqueous methanol solution (H_2O/MeOH 1:5 v/v). The reaction mixture was heated at reflux for 18 h, cooled, and then filtered through Celite to afford a dark red/orange filtrate. The solvent was removed in vacuo and then passed through a silica column (acetone/MeOH/$KNO_{3(aq)}$ 2:1:1). The sample was passed through a silica column (MeOH/$CHCl_3$ 3:1) a second time, and 56 mg of a red-purple product was obtained after recrystallization from CH_2Cl_2 and hexanes (yield = 14%). ^{1}H NMR (CD_3OD): 6.42 (dd, 1H, ^3J = 7 Hz, ^4J = 1 Hz), 6.79 (td, 1H, ^3J = 7 Hz, ^4J = 1 Hz), 6.89 (td, 1H, ^3J = 7 Hz, ^4J = 1 Hz), 7.19−7.28 (m, 3H), 7.31, (dd, 1H, ^3J = 6 Hz, ^4J = 2 Hz), 7.46 (ddd, 1H, ^3J = 7 Hz, 5 Hz, ^4J = 1 Hz), 7.58 (d, 1H, ^3J = 6 Hz, ^4J = 1 Hz), 7.72−7.91 (m, 7H), 8.02 (ddd, 1H, ^3J = 8 Hz, 8 Hz, ^4J = 1 Hz), 8.10 (ddd, 1H, ^3J = 5 Hz, ^4J = 2 Hz, ^5J = 1 Hz), 8.41 (d, 1H, ^3J = 8 Hz), 8.45 (d, 1H, ^4J = 1 Hz), 8.45 (d, 1H, ^3J = 8 Hz), 8.51 (d, 1H, ^3J = 8 Hz), 8.61 (d, 1H, ^3J = 8 Hz). ESI-MS: m/z 612.0 (calcd for $\{M^+\}$ 612.1) ^{13}C NMR (CD_3OD with 1 drop of NaOD): 194, 172, 169, 159, 159, 158, 157, 156, 151, 151, 151, 150, 147, 146, 138, 136, 136, 135, 135, 130, 128, 128, 127, 127, 125, 125, 125, 124, 124, 123, 122, 119. HRMS (MALDI-TOF): m/z = 612.09902 [(M)+] (calcd for $C_{32}H_{24}N_5O_2Ru^+$: m/z = 612.097661).

[Ru(dcbpy)$_2$(ppy)]PF$_6$ (5c). To a flask containing 99 mg (0.17 mmol) of [Ru(ppy)(CH_3CN)$_4$]PF_6, 87 mg (0.36 mmol) of 2,2′-bipyridine-4,4′-dicarboxylic acid, and 29 mg (0.73 mmol) of sodium hydroxide was added 30 mL of degassed aqueous methanol solution (H_2O/MeOH 1:5 v/v). The reaction mixture was then refluxed for 3 h. The solvent was then removed in vacuo to afford a dark purple solid, which was purified using silica column chromatography (MeOH/$CHCl_3$ 3:1). The dark purple fraction was isolated, reconstituted in 20 mL of MeOH and then drawn out of solution using 100 mL of Et_2O to afford 104 mg of a purple solid (yield = 80.0%). ^{1}H NMR (CD_3OD plus a drop of NaOD): 6.39 (dd, 1H, ^3J = 7 Hz, ^4J = 1 Hz), 6.81 (dt, 1H, ^3J = 7 Hz, ^4J = 1 Hz), 6.89 (dt, 1H, ^3J = 7 Hz, ^4J = 1 Hz), 6.95 (ddd, 1H, ^3J = 7 Hz, 6 Hz, ^4J = 1 Hz), 7.54 (d, 1H, ^3J = 5 Hz), 7.60 (dd, 1H, ^3J = 7 Hz, ^4J = 1 Hz), 7.63 (dd, 1H, ^3J = 6 Hz, ^4J = 2 Hz), 7.65 (dd, 1H, ^3J = 6 Hz, ^4J = 2 Hz), 7.70 (dt, 1H, ^3J = 7 Hz, ^4J = 2 Hz), 7.76 (d, 1H, ^3J = 6 Hz), 7.83−7.87 (m, 3H), 7.88(dt, 1H, ^3J = 5 Hz, ^4J = 1 Hz), 8.06 (d, 1H, ^3J = 8 Hz), 8.13 (d, 1H, ^3J = 6 Hz), 8.86 (s, 1H), 8.87 (s, 1H), 8.94 (s, 1H), 9.02 (s, 1H). ESI-MS: m/z 744.01 (calcd for $RuC_{35}H_{21}N_5O_8$ 744.07) Anal. Calcd for $C_{35}H_{24}F_6N_5O_8PRu$ + 5H_2O: C, 42.95; H, 3.50; N, 7.16. Found: C, 42.93; H, 3.67; N, 7.27.

[Ru(bpy)$_2$(bhq)]PF$_6$ (6). In accord with a previously described procedure,[17] a flask containing 232 mg (0.446 mmol) of Ru(bpy)$_2$Cl$_2$, 204 mg (1.05 mmol) of $AgBF_4$, and 242 mg (1.35 mmol) of Hbhq in 30 mL of dichloromethane was stirred at reflux for 19 h. After the solution was cooled, filtered through Celite, and concentrated to 5 mL, 200 mL of hexanes was added, and the solution was left to stand at 4 °C overnight to afford a dark red-purple solid. The solid purified by column chromatography (silica; MeCN/$KNO_{3(aq)}$ 7:1), followed by anion exchange with a saturated aqueous NH_4PF_6 methanolic solution. The precipitate was filtered and washed with ether (3 × 15 mL) to afford 57.0 mg of the product (yield = 17.0%). ^{1}H NMR (CD_3CN): 6.69 (dd, 1H, ^3J = 7 Hz, ^4J = 1 Hz), 6.95 (d, 1H, ^3J = 9 Hz), 7.03−7.07 (m, 1H), 7.10 (d, 1H, ^3J = 9 Hz), 7.27 (m, 3H), 7.43 (d, 1H, ^3J = 8 Hz), 7.48 (ddd, 1H, ^3J = 7 Hz, 6 Hz, ^4J = 1 Hz), 7.64 (d, 1H, ^3J = 6 Hz), 7.74 (m, 3H), 7.87 (m, 4H), 8.01−8.04 (m, 2H), 8.22 (d, 1H, ^3J = 8 Hz), 8.31 (d, 1H, ^3J = 8 Hz), 8.37 (m, 2H), 8.50 (d, 1H, ^3J = 8 Hz). ESI-MS: m/z 592.0 (calcd for $\{M^+\}$ 592.1) Anal. Calcd for $C_{33}H_{24}F_6N_5PRu$ + CH_2Cl_2 + CH_3OH: C, 49.25; H, 3.54; N, 8.20. Found: C, 49.75; H, 3.33; N, 7.70. HRMS (MALDI-TOF): m/z = 592.107848 [(M)+] (calcd for $C_{33}H_{24}N_5Ru^+$: m/z = 592.10686).

[Ru(tpy)(dpb)]PF$_6$ (7). Following a previously described procedure,[38] a flask containing 37.1 mg (84.2 μmol) of Ru(tpy)Cl_3 and 19.4 mg (83.5 μmol) of Hdpb was charged with 12 mL of an aqueous methanol solution (MeOH/H_2O 5:1 v/v) containing

4 drops of *N*-ethylmorpholine and stirred at reflux for 4 h. The solution was cooled to room temperature and filtered. The purple filtrate was then stirred with excess NH_4PF_6 for 5 min, followed by the removal of solvent in vacuo. The resultant purple solid was dissolved in a minimal amount of THF and loaded onto a silica column (CH_2Cl_2/Et_2O 9:1 v/v). The red band was isolated and recrystallized from CH_2Cl_2 and hexanes to yield 24.2 mg of a black crystalline product (yield = 40.5%). ^{1}H NMR (CD_3CN): δ 6.65 (ddd, 2H, ^3J = 6 Hz, ^3J = 6 Hz, ^4J = 1 Hz), 6.95 (dt, 2H, ^3J = 7), 7.02 (d, 2H, ^3J = 5 Hz), 7.11 (d, 2H, ^3J = 5 Hz), 7.46 (t, 1H, ^3J = 8 Hz), 7.60 (dt, 2H, ^3J = 8 Hz, ^4J = 1 Hz), 7.69 (dt, 2H, ^3J = 8 Hz, ^4J = 1 Hz), 8.14 (d, 2H, ^3J = 8 Hz), 8.24 (t, 1H, ^3J = 8 Hz), 8.25 (d, 2H, ^3J = 8 Hz), 8.42 (d, 2H, ^3J = 8 Hz), 8.74 (d, 2H, ^3J = 8 Hz). ESI-MS: *m*/*z* 566.13 (calcd for {M}$^+$ 566.09). Anal. Calcd for $C_{31}H_{22}F_6N_5PRu$: C, 52.40; H, 3.12; N, 9.86. Found: C, 52.18; H, 3.38; N, 9.40.

[Ru(tpy)(pbpy)]PF$_6$ (8). Following a previously described procedure,[13] a flask containing 75.0 mg (170 μmol) of Ru(tpy)Cl_3 and 39.8 mg (170 μmol) of pbpy was charged with 4 drops of *N*-ethylmorpholine in 24 mL of aqueous methanol (5:1 MeOH/H_2O v/v). The reaction mixture was stirred for 4 h at reflux, and then filtered after being cooled to room temperature. Excess NH_4PF_6 was added to the filtrate and stirred for 5 min, followed by removal of the solvent in vacuo. The resultant purple solid was dissolved in a minimum volume of THF and passed through a silica column (CH_2Cl_2/THF/Et_2O 5:5:2 v/v). The purple band was isolated and recrystallized from CH_2Cl_2 and hexanes to afford 50.8 mg of a dark purple product (yield = 42.0%). ^{1}H NMR (CD_3CN): δ 5.68 (d, 1H, ^3J = 8 Hz), 6.51 (t, 1H, ^3J = 8 Hz), 6.73 (dt, 1H, ^3J = 8 Hz, ^4J = 1 Hz), 7.05 (dt, 3H, ^3J = 8 Hz, ^4J = 1 Hz), 7.43 (m, 3H), 7.75 (dt, 2H, ^3J = 8 Hz, ^4J = 1 Hz), 7.81 (dd, 1H, ^3J = 8 Hz, ^4J = 1 Hz), 7.86 (dt, 1H, ^3J = 8 Hz, ^4J = 1 Hz), 8.04 (t, 1H, ^3J = 8 Hz), 8.07 (t, 1H, ^3J = 8 Hz), 8.23 (dd, 1H, ^3J = 8 Hz, ^4J = 1 Hz), 8.40 (dd, 3H, ^3J = 8 Hz, ^4J = 1 Hz), 8.43 (d, 1H, ^3J = 8 Hz), 8.59 (d, 2H, ^3J = 8 Hz). ESI-MS: *m*/*z* 566.08 (calcd for {M}$^+$ 566.09). Anal. Calcd for $C_{31}H_{22}F_6N_5PRu$: C, 52.40; H, 3.12; N, 9.86. Found: C, 52.24; H, 3.42; N, 9.66.

[Ru(tpy)(pbpy-CO$_2$H)]PF$_6$ (8a). A flask containing 75.0 mg (170 μmol) of Ru(tpy)Cl_3, 39.8 mg (170 μmol) of pbpy-CO_2H, and 4 drops of *N*-ethylmorpholine in 24 mL of a degassed aqueous methanol solution (H_2O/MeOH 1:5 v/v) was stirred at reflux for 4 h. After the purple solution was cooled to room temperature and filtered, excess NH_4PF_6 was added to the filtrate and stirred for 5 min. The solvent was removed in vacuo and the resultant purple solid was redissolved in THF and passed through a silica column (MeCN:sat KNO_3 7:3 v/v). The purple band was isolated and the solvent was removed in vacuo. The purple solid was dissolved in 400 mL of hot water, and the product was precipitated upon addition of excess KPF_6. The solid was filtered, washed with water and recrystallized from CH_2Cl_2 and hexanes to afford 40.8 mg of a deep purple crystalline product (yield = 35.6%). ^{1}H NMR (CD_3CN): δ 5.74 (d, 1H, ^3J = 8 Hz), 6.54 (dt, 1H, ^3J = 8 Hz, ^4J = 1 Hz), 6.75 (dt, 1H, ^3J = 8 Hz, ^4J = 1 Hz), 7.02 (m, 3H), 7.42 (d, 1H, ^3J = 8 Hz), 7.47 (d, 1H), 7,74 (dt, 2H, ^3J = 8 Hz, ^4J = 1 Hz), 7.85 (dt, 1H, ^3J = 8 Hz, ^4J = 1 Hz), 7.93 (d, 2H, ^3J = 8 Hz), 8.07 (t, 1H, ^3J = 8 Hz), 8.40 (d, 2H, ^3J = 8 Hz), 8.61 (d, 3H, ^3J = 8 Hz), 8.74 (s, 1H), 8.94 (s, 1H). ESI-MS: *m*/*z* 610.05 (calcd for {M}$^+$ 610.08). Anal. Calcd for $C_{32}H_{22}F_6N_5O_2PRu$+1.33 C_6H_{14}: C, 55.25; H, 4.71; N, 8.05. Found: C, 55.60; H, 4.43; N, 8.14.

[Ru(tpy)(ppy)Cl] (9). A flask containing 86.3 mg (0.196 mmol) of Ru(tpy)Cl_3, 35.0 μL (0.245 mmol) of Hppy, and 4 drops of *N*-ethylmorpholine in 18 mL of an aqueous methanol solution (H_2O/MeOH 1:5 v/v) was stirred for 4 h at reflux. The solution was cooled to room temperature and then filtered. The dark purple precipitate was washed with 3 × 15 mL of Et_2O to remove excess Hppy. The solid was dissolved in MeOH and filtered to remove impurities. The solvent was then removed in vacuo to yield a pure dark purple solid to afford 25.2 mg (yield = 24.5%) of the product. ^{1}H NMR (CD_3OD; solution contains one drop of a saturated methanolic solution of ascorbic acid to avoid aerial oxidation): δ 5.62 (d, 1H), 6.35 (t, 1H), 6.56 (t, 2H), 7.26 (m, 2H), 7.60 (m, 1H), 7.67 (m, 2H), 7.83 (t, 2H), 7.93 (t, 1H), 7.99 (t, 1H), 8.23 (d, 1H), 8.39 (d, 2H), 8.48 (d, 2H), 9.31 (s, 1H). Anal. Calcd for $C_{26}H_{19}ClN_4Ru$ + H_2O: C, 57.62; H, 3.91; N, 10.34. Found: C, 57.81; H, 3.72; N, 10.27. ESI-MS: *m*/*z* 566.13 (calcd for {M}$^+$ 566.09).

[Ru(tpy)(bhq)Cl] (10). A flask containing 100 mg (0.228 mmol) of Ru(tpy)Cl_3, 61.2 mg (0.341 mmol) of Hbhq, and 4 drops of *N*-ethylmorpholine in 18 mL aqueous methanol (5:1 MeOH/H_2O v/v) was stirred for 4 h at reflux. The solution was cooled to room temperature and then filtered. The purple precipitate was washed with Et_2O (3 × 15 mL) to remove excess Hbhq, then reconstituted in MeOH and filtered. Solvent was removed in vacuo to afford 17.1 mg of a dark purple solid (yield = 13.7%). ^{1}H NMR (CD_3OD; solution contains one drop of a saturated methanolic solution of ascorbic acid to avoid aerial oxidation): δ 5.88 (s, 1H), 6.75 (t, 1H), 7.01 (d, 1H), 7.11(d, 2H), 7.50 (d, 2H), 7.72 (d, 1H), 7.78 (t, 3H), 7.96 (t, 2H), 8.39 (d, 2H), 8.51 (d, 3H), 9.58 (s, 1H). ESI-MS: *m*/*z* 547.95 (calcd for {M}$^+$ 548.03), 513.03 (calcd for {M$^+$ − Cl$^-$} 513.07). Anal. Calcd for $C_{28}H_{19}ClN_4Ru$ + CH_3OH: C, 60.05; H, 4.00; N, 9.66. Found: C, 60.27; H, 3.62; N, 10.04.

Physical Methods. Electrochemical measurements were performed under anaerobic conditions with a Princeton Applied Research VersaStat 3 potentiostat using dry solvents, Pt working and counter electrodes, a Ag pseudoreference electrode, and 0.1 M NBu_4BF_4 supporting electrolyte. Potentials were initially referenced to an internal ferrocene (Fc) standard; however, potentials reported herein are referenced to a normal hydrogen electrode (NHE) on the premise that the [Fc]/[Fc]$^+$ couple occurs at +0.640 V versus NHE in MeCN.[41] ^{1}H spectra were recorded in dry deuterated solvents at 400 MHz on a Bruker AV 400 instrument at ambient temperatures unless otherwise stated. Chemical shifts (δ) are reported in parts per million (ppm) from high- to low-field and referenced to residual non-deuterated solvents. Standard abbreviations indicating multiplicity are used as follows: vbr = very broad; d = doublet; m = multiplet; s = singlet; t = triplet. Electronic spectroscopic data were collected on MeCN solutions using a Cary 5000 UV−vis spectrophotometer (Varian). Steady-state emission spectra were obtained at room temperature using an Edinburgh Instruments FLS920 Spectrometer equipped with a Xe900 450W steady state xenon arc lamp, TMS300-X excitation monochromator, TMS300-M emission monochromator, Hamamatsu R2658P PMT detector and corrected for detector response. Elemental analysis (EA) was performed on a Perkin-Elmer Series II CHNS/O Analyzer 2400, electrospray ionization mass spectrometry (ESI-MS) data were collected on a Bruker Esquire 3000 ion-trap detector (target mass = 600 *m*/*z*; drying temperature = 300 °C; flow rate = 0.7 L/min, nebulizer gas pressure = 7 PSI), and high resolution mass spectrometry (HR-MS) were collected on a Bruker Autoflex III MALDI-TOF.

DFT Calculations. Density functional theory (DFT) calculations were carried out using B3LYP (Becke's three-parameter exchange functional (B3) and the Lee−Yang−Parr correlation functional (LYP)) and the LanL2DZ basis set. All geometries were fully optimized in the ground states (closed-shell singlet S_o). Time-dependent density functional theory (TD-DFT) calculations were performed with a spin-restricted formalism to examine low-energy excitations at the ground-state geometry. All calculations were carried out with the Gaussian 03W software package.

(41) Pavlishchuk, V. V.; Addison, A. W. *Inorg. Chim. Acta* **2000**, *298*, 97–102.

Results

Synthesis and Characterization. The syntheses of cyclometalated complexes **5**−**10** are relatively onerous compared to their polypyridyl-based congeners because of the requisite C−H bond activation step. Nonetheless, the preparation of the target complexes can still be achieved under fairly mild reaction conditions. A typical procedure involves the initial coordination of the polypyridyl ligand to the Ru center, followed by addition of the respective cyclometalating ligand (e.g., *C^N*, *N^C^N* or *C^N^N*), often in the presence of a base. Anion exchange reactions were carried out for all cationic complexes (except **5b**) so that microcrystalline samples could be isolated; all analyses were carried out on the PF_6^- salts of the cationic complexes **1**−**8** (the NO_3^- salt was isolated for **5b**). The yields of the cyclometalated complexes are substantially lower compared to the polypyridyl analogues, which is due, in part, to the additional purification steps required to separate the desired product from the common homoleptic byproducts (e.g., $[Ru(bpy)_3]^{2+}$, $[Ru(tpy)_2]^{2+}$) or the non-cyclometalated derivatives. Achieving reasonable yields demands halide abstraction prior to cyclometalation in cases where $Ru(bpy)_2Cl_2$ is used as the synthon. This step is not compulsory when $Ru(tpy)Cl_3$ is treated with tridentate ligands such as $pbpy^-$ or dpb^-.

The identities of the complexes were verified by ESI-MS and ^{1}H NMR spectroscopy. ^{1}H NMR spectroscopy is a convenient tool for monitoring these reactions owing to the fact that cyclometalation has a dramatic influence on the proton *ortho* or *para* to the C_{aryl} atom bound to the Ru center.[12] In the case of **5**, for instance, the proton resonance *ortho* to the C_{aryl} atom at 6.41 ppm is shifted upfield by 1.34 ppm relative to the analogous proton in **1** at 7.75 ppm (Figure 3). The other protons situated on the phenyl ring are also moved upfield, but to a lesser extent. The spectrum of **5** is more complicated than that of **1** because of the collapse of D_3 symmetry; thus, a 2D COSY experiment was used to aid in the assignment of the proton signals. A more pronounced effect is observed in the tridentate series: the signal corresponding to the resonance adjacent to the organometallic bond in **8** is found at 5.68 ppm (an upfield shift of 1.66 ppm relative to **3**), with the *meta* and *para* protons at 6.52 and 6.73 ppm, respectively. The upfield proton is more shielded in **8** than in **5** because of the interaction with the central pyridine ring of the proximate tpy ligand. The same degree of shielding of the aromatic protons is not observed for **7** because there are no protons *ortho* to the C_{aryl} atom bound to the Ru center; however, the signal *para* to this C_{aryl} atom is drawn upfield by 0.96 ppm relative to the proton at the 4′ position of the tpy ligand in **3**. Special care must be taken for the acquisition of ^{1}H NMR spectra of the $[Ru(tpy)(C^N)Cl]^+$ compounds because of their susceptibility to oxidation in solution, but we were able to suppress adventitious oxidation by adding ascorbic acid to the solution to record satisfactory spectra for both **9** and **10**. These spectra again reveal upfield aromatic protons at 5.62 and 5.88 ppm, respectively, to indicate that cyclometalation has occurred. The spectra also indicate that of the two possible isomers present in solution, only the isomer with the Ru−C_{aryl} bond *trans* to the Cl^- ligand is observed for both **9** and **10** (which was previously verified by single-crystal X-ray crystallography[42]). The shielding of the proton *ortho* to the Ru−C_{aryl} bond by the tpy ligand in **9** leads to a resonance at 5.62 ppm, while the proton *ortho* to the Ru−N bond in the same ligand is pushed downfield (to 9.31 ppm) because of the interaction with the halide ligand.

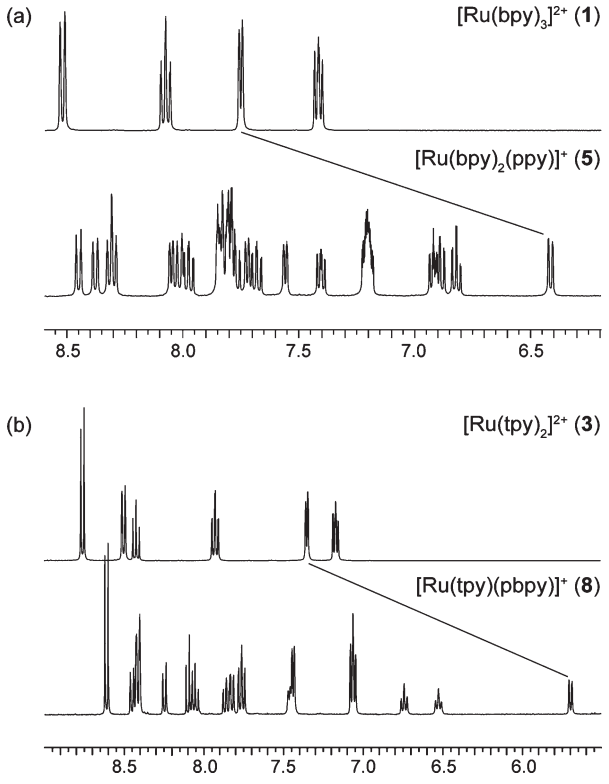

Figure 3. ^{1}H NMR spectra for **1**, **5**, **3**, and **8** in CD_3CN solutions at ambient temperatures. Solid line tracks shift of proton *ortho* to Ru−C(N) bond.

Electrochemical Behavior

The electrochemical properties of **1**−**10** were examined by cyclic voltammetry; the observed redox couples are collected in Table 1. Most compounds exhibit well-resolved redox couples ($i_{p,a}/i_{p,c} \approx 1$) over the −2 to +2 V (vs NHE) range, and resting potentials occurred within 0.5 V of 0 V versus NHE; representative cyclic voltammograms are provided in Figure 4. The redox behavior of **1** (which has been presented in detail elsewhere[6,43]) consists of a reversible metal-based oxidation process at +1.52 V and a ligand-based reduction wave at −1.09 V. Both oxidation and reduction waves for **5**, however, are shifted substantially to more negative values, with observed oxidation and reduction signals at +0.70 and −1.36 V, respectively.[16] As in the case of the non-cyclometalated congeners, the oxidation process is assigned as a $Ru^{II/III}$ couple, and the reduction process is confined to the polypyridyl ligand. The incorporation of the σ-bond leads to a shift of the oxidation and reduction processes by about −0.8 V and −0.3 V, respectively. These shifts are ascribed to the additional electron density on the metal center and the disparity of the overall charge of the complexes (e.g., **1** is

(42) Hadadzadeh, H.; DeRosa, M. C.; Yap, G. P. A.; Rezvani, A. R.; Crutchley, R. J. *Inorg. Chem.* **2002**, *41*, 6521–6526.
(43) Balzani, V.; Juris, A.; Barigelletti, F.; Belser, P.; Von Zelewsky, A. *Sci. Pap. Inst. Phys. Chem. Res.* (*Jpn.*) **1984**, *78*, 78–85.

Table 1. Electrochemical and Electronic Spectroscopy Data for Compounds **1**−**10**[a]

compound	$E_{1/2}$ (V vs NHE) E_{ox1}	E_{red1}	E_{red2}	λ_{max}[b] (nm)	ε ($\times 10^4$ M^{-1} cm^{-1})	λ_{em}[c] (nm)
			$[Ru(bpy)_2(L)]^z$ Series			
$[Ru(bpy)_3]^{2+}$ (**1**)	+1.52	−1.09	−1.29[d]	451	1.4	615
$[Ru(bpy)_2(phen)]^{2+}$ (**2**)	+1.52	−1.08	−1.28[e]	449	1.6	612
$[Ru(bpy)_2(ppy)]^+$ (**5**)	+0.70	−1.36	−1.62	546	1.0	800
$[Ru(bpy)_2(pba)]^+$ (**5a**)	+0.82	−1.35	−1.62	530	1.0	760
$[Ru(bpy)_2(ppy\text{-}CO_2H)]^+$ (**5b**)	+0.67	−1.36	−1.62	554	1.1	807
$[Ru(dcbpy)_2(ppy)]^+$ (**5c**)	—[f]	—[f]	—[f]	575	—[f]	—[f]
	(+0.76[g])			(562[g])	(1.0[g])	(809[g])
$[Ru(bpy)_2(bhq)]^+$ (**6**)	+0.73	−1.34	−1.58	543	0.84	784
			$[Ru(tpy)(L)]^z$ Series			
$[Ru(tpy)_2]^{2+}$ (**3**)	+1.52	−1.02	−1.27	476	1.5	
$[Ru(tpy)(dpb)]^+$ (**7**)	+0.75	−1.32	−1.76[h]	500	1.2	705
$[Ru(tpy)(pbpy)]^+$ (**8**)	+0.73	−1.40	−1.68	513	1.3	708
$[Ru(tpy)(pbpy\text{-}CO_2H)]^+$ (**8a**)	+0.86	−1.39	−1.68[h]	515	1.2	716
			$[Ru(tpy)(L)Cl]^z$ Series			
$[Ru(tpy)(bpy)Cl]^+$ (**4**)	+1.05	−1.20	−1.33	482	0.96	729
$[Ru(tpy)(ppy)Cl]$ (**9**)	+0.46[i]	−1.40[i]	−1.50[i]	541[j]	0.34[j]	782[j]
$[Ru(tpy)(bhq)Cl]$ (**10**)	+0.48[i]	−1.37[i]	−1.53[i]	537[j]	0.71[j]	725[j]

[a] All data recorded in MeCN at 298 K unless otherwise specified; counterion is PF_6^- for all cationic complexes except **5b**, which was measured as the NO_3^- salt; all values in table measured in our laboratories. [b] Only the lowest-energy absorption band (λ_{max}) is listed. [c] All data collected in deaerated solvent at ambient temperatures. [d] $E_{1/2}$ (red3) is observed at −1.53 V. [e] Poorly resolved. [f] Poor solubility precluded collection of redox potentials, ε values, and λ_{em}. [g] Corresponds to monodeprotonated form (i.e., {**5c**-H^+}); data recorded in MeOH (solvent correction applied by correlating $E_{1/2}$ (ox) of **5** measured in MeOH against $[Fc]/[Fc]^+$). [h] Irreversible ($E_{p,c}$ is reported). [i] Measured in DMF. [j] Measured in MeOH.

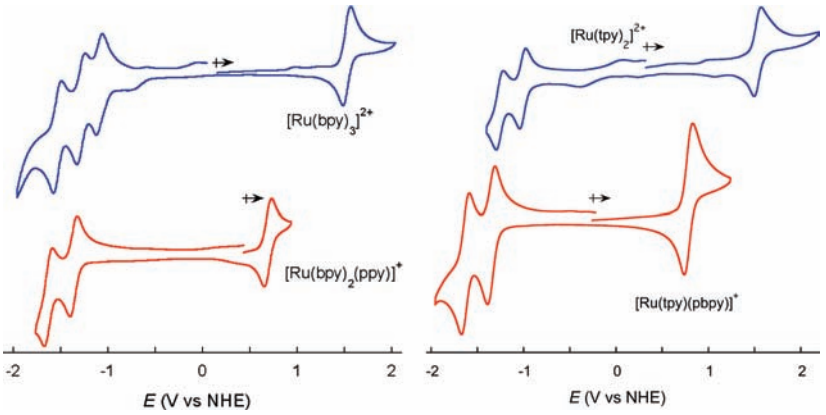

Figure 4. Cyclic voltammograms of bidentate complexes $[Ru(bpy)_3](PF_6)_2$ (**1**) and $[Ru(bpy)_2(ppy)]PF_6$ (**5**), and tridentate complexes $[Ru(tpy)_2](PF_6)_2$ (**3**) and $[Ru(tpy)(pbpy)]PF_6$ (**8**) in acetonitrile at 298 K (scan rate = 100 mV/s).[16,21] Peak potentials (vs NHE) for the redox couples are indicated in Table 1.

dicationic, while **5** is monocationic). The shift of the reduction potentials upon cyclometalation is a consequence of enhanced π-backbonding to the pyridyl rings resulting from the increased electron density at the metal center.[14] These same trends are observed for each independent series, $[Ru(bpy)_2(L)]^z$, $[Ru(tpy)(L)]^z$, and $[Ru(tpy)(L)Cl]^z$.

The diminution of electron density at the metal upon attaching a $-CO_2H$ group to the ppy^- ligand is corroborated by a shift in oxidation potential of **5a** to more positive values with virtually no effect on the first reduction potential relative to **5**. The first oxidation wave for **5b**, on the other hand, is only slightly affected, while the first reduction wave remains static. These results, collectively, are consistent with electron density in the HOMO partially delocalized over both the phenyl ring and the metal center, and the first reduction wave is associated with the pyridyl ligands (vide infra). Electrochemical data for **5c** could not be directly measured because of poor solubility in organic solvents. The cyclic voltammogram for the monodeprotonated form of **5c** in MeOH, however, revealed a single redox process over the −1 to +1 V range; namely, a reversible oxidation couple at +0.76 V. Taking into account a single H^+ shifts the oxidation potential by about +0.2 V in related systems,[30] the first oxidation potential of **5c** likely occurs at about +0.96 V. The higher oxidation potential of **5c** relative to **5** is consistent with the $-CO_2H$ anchoring groups reducing the electron density at the metal.

The reduction and oxidation waves do not vary significantly over the series **1**−**3**, but the Cl^- ligand present in **4** induces a negative shift in all observed thermodynamic potentials.[6] The effect of attaching a strongly σ-donating aryl group to the metal already ligated to the π-donating Cl^- produces the lowest oxidation potentials of all species measured in this study. For instance, the oxidation potentials for **9** and **10** are about 0.6 V lower than that of **4**, and about

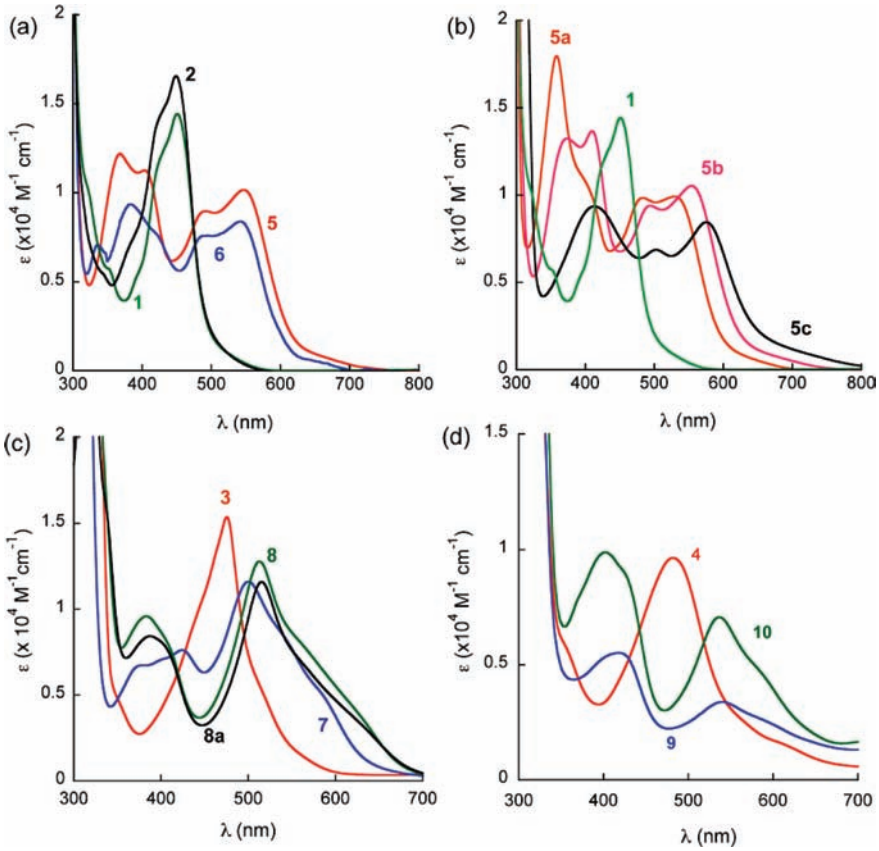

Figure 5. Electronic absorbance spectra for the (a and b) $[Ru(bpy)_2(L)]^z$, (c) $[Ru(tpy)(L)]^z$ and (d) $[Ru(tpy)(L)(Cl)]^z$ series recorded in MeCN at ambient temperature.

1.1 V lower than the complexes containing six Ru−N bonds (i.e., **1**−**3**).

Electronic Spectroscopy

The UV−vis absorption spectra for compounds **1**−**10** are provided in Figure 5; the maxima corresponding to the lowest-energy absorption bands and the corresponding emission data are listed in Table 1. A common feature over the entire series is the presence of intense bands in the ultraviolet region between 300−350 nm, which are assigned as spin-allowed $^1(\pi-\pi^*)$ ligand transitions.[6] Examination of the lower energy bands reveals pronounced differences in the absorption profiles; *namely*, a substantial bathochromic shift and a larger spectral envelope upon cyclometalation (there are also extra features below 300 nm ascribed to intraligand $\pi-\pi^*$ transitions). For the bidentate series, the spectral maxima of the lowest-energy transitions for **5** and **6** are red-shifted by about 95 nm compared to **1** and **2**. The lowering of the symmetry upon incorporation of a Ru−C σ-bond results in transitions that lead to a broader absorption envelope. Within the tridentate series, **7** and **8** are only shifted to longer wavelengths by 24−39 nm compared to **3**, but the molar extinction coefficients, which are on the order of 15,000 M^{-1} cm^{-1}, are not diminished to the same extent as in the bidentate series. A feature that emerges in the spectra of the cyclometalated compounds is the set of intense bands over the 350−450 nm range. The molar extinction coefficients of these bands are consistent with significant MLCT character, and are ascribed to the population of excited states involving the cyclometalated ligands; the MLCT bands at >500 nm have excited states localized primarily to the polypyridyl ligands (vide infra).

The spectra of the $[Ru(tpy)(L)Cl]^z$ series reveal the dramatic effect of Cl^- ligation on the electronic structure of these compounds. The λ_{max} value for **4** is red-shifted by 30−57 nm compared to **1**−**3**, a consequence of a destabilized HOMO because of the repulsion of the filled metal d orbitals with the filled p orbitals of the halide ligand. Substitution of bpy by either ppy^- or bhq^- produces an additional bathochromic shift of about 30 nm. The ε values of neutral complexes **9** and **10** are relatively low to that of **4**; however, we caution that the data may be affected by the low solubility of these complexes. Like the other cyclometalated complexes, intense bands are observed at 350—450 nm. In contrast to the $[Ru(tpy)(L)]^z$ series, however, these transitions are more intense than the lowest-energy bands. This is aligned with the assignment that the lowest-energy excitation process involves excited states localized to the tpy ligand, while the transitions at about 400 nm involve excited-states associated with ppy^- or bhq^-.

There are distinct spectral changes for the complexes containing the $-CO_2H$ substituents that are consistent with the assignment of the transitions over the 350−700 nm range. In the case of **5a**, for instance, the $-CO_2H$ group results in a blue-shift of the lowest-energy band by 16 nm, and the band at about 400 nm by 8 nm. Both of these MLCT bands are red-shifted in the cases of **5b** and **5c**, with the lowest-energy transition observed for **5c** (λ_{max} at 575 nm). These trends are consistent with a LUMO delocalized primarily over the polypyridyl ligands, and a HOMO with electron density delocalized over both the metal and the aryl ring of the cyclometalating ligand (vide infra). Because an accurate ε

value could not be obtained for **5c** due to solubility issues in a range of solvents, we provide data corresponding to the monodeprotonated form of **5c** for comparison (λ_{max} = 562 nm).

Excitation at wavelengths defined by the absorption maximum of the lowest-energy excited states produced emission signals that were very weak for all cyclometalated compounds in this study. The room temperature spectra indicate a substantial Stokes shift for the entire series accompanied with poor quantum yields. According to the energy gap law, the destabilization of the HOMO provides non-radiative pathways to the ground state that suppresses fluorescence, a feature common to cyclometalated compounds.[18,44−46] Studies examining the factors that dictate the photophysics of these compounds are underway.

DFT Calculations

B3LYP/LanL2DZ DFT calculations were carried out on all compounds to aid in the determination of the electronic structure, while TD-DFT calculations on optimized geometries in MeCN were employed to model the corresponding absorption spectra. The correlation of theory to the UV−vis spectra shown in Figure 5 is confined to transitions occurring over the 350−700 nm range. The low-energy transitions for the polypyridyl and cyclometalated compounds are blue-shifted by about 30 and 50 nm, respectively, relative to the experimental data; however, trends in calculated spectra are aligned with experimental data (see Supporting Information). All reported values have been converted to a thermodynamic scale of V versus NHE (with the assumption that 0 V vs NHE corresponds to a vacuum level of −4.5 eV[3]).

The experimental data and TD-DFT results indicate a number of transitions within the absorption manifold of the cyclometalated complexes. This broad envelope arises primarily because (i) a set of π^* orbitals associated with the cyclometalated ligand are located at slightly higher energies than those of the polypyridyl ligands that comprise the LUMO; and (ii) there is a breakdown in degeneracy of the d orbitals, which comprise the highest-energy occupied orbitals, in the presence of a single Ru−C bond. The electron density of the HOMO for all cyclometalated complexes is found primarily on the metal, but there is also significant cyclometalating ligand character. Cognizant of this feature, we broadly classify all electronic transitions that emanate from a metal-based HOMO with partial ligand character to a ligand-based π^* orbital as a MLCT transition for the sake of brevity.

In the case of **5**, the HOMOs follow the order d_{xy} (HOMO−2) < d_{yz} (HOMO−1) < d_{xz} (HOMO) (Figure 6);[14] the unoccupied metal orbitals reside significantly higher in energy relative to the polypyridyl congeners. The LUMO and LUMO+1 levels are delocalized over the π^* system of both bpy ligands, while the π^* orbitals of all three ligands contribute to the LUMO+2 level (which lies 0.75 eV above the LUMO). The lowest-energy maximum in the UV−vis spectrum of **5** is therefore assigned as a MLCT process involving Ru→bpy transitions, while the features at about 400 nm involve an excited state delocalized over the π^* system of the ppy^- ligand. The presence of bhq^- in place of the ppy^- ligand has no notable effect on the electronic structure of the ground- and excited-states.

The only structural difference between **5** and **5a** is the presence of a carboxylic acid attached to the phenyl ring of the ppy^- ligand, which results in the stabilization of the HOMO by +0.10 eV. With the $-CO_2H$ group attached to the pyridine ring in **5b**, however, the π^* orbitals of the pyridine portion of the ppy−CO_2H ligand are pulled to lower energies than those associated with the bpy ligands. Because the electron density of the LUMO in **5** is delocalized over the π^* of the bpy ligands, electron-withdrawing substituents on these ligands are most effective in lowering the LUMO. Consequently, **5c** provides the most red-shifted absorption profile of all the compounds measured in this study. We also note that the ground-state oxidation potential of **5c** is calculated to be about +1.0 V − a value that resonates with the oxidation potential of +0.96 V that we proposed in the Electrochemistry Section.

An examination of the $[Ru(tpy)(L)]^z$ series reveals that the HOMO electron density of **3** is localized primarily on the metal d_{xy} orbital (degenerate d_{xz} and d_{yz} orbitals lie slightly lower in energy), with some ligand character distributed over both tpy ligands (Figure 7). The substitution of a single tpy ligand with either $pbpy^-$ or dpb^- affects the ordering of the d orbitals and destabilizes the σ^* orbitals substantially. We again note that there is significant ligand contribution (up to 50%) to the HOMO levels.[32] The principal contribution to the lowest-energy band centered at 500 nm involves HOMO−1/HOMO−2 → LUMO/LUMO+1 transitions that correspond to the promotion of electrons from degenerate d_{yz} and d_{xy} orbitals to the tpy ligand. The shoulder at shorter wavelengths is ascribed to a Ru→dpb^- MLCT process; that is, HOMO−1 → LUMO+2. The features occurring between 350 and 450 nm are assigned as MLCT transitions involving the dpb^- ligand. The reduced symmetry of **8** forces the Ru−C_{aryl} σ-bond to be oriented perpendicular to the z-axis, which affects the degeneracy of the energy levels and increases the number of observed transitions. This arrangement results in the reordering of the highest occupied metal orbitals to follow d_{xz} (HOMO−2) < d_{yz} (HOMO−1) ~ d_{xy} (HOMO). The experimental UV−vis spectrum indicates two features on the low-energy tail of the MLCT band: the lower energy transition at 630 nm is predominantly a Ru→tpy CT process, while the features at 565 and 513 nm are dominated by transitions from the Ru center to the tpy ligand and the pyridine rings of the $pbpy^-$ ligand. Higher energy transitions around 400 nm are assigned as MLCT bands to the orbitals delocalized over the entire $pbpy^-$ ligand. The $-CO_2H$ substituent on the $pbpy^-$ ligand of **8a** stabilizes the orbital centered on the cyclometalating ligand such that the electron density of the LUMO is delocalized over the $(pbpy\text{-}CO_2H)^-$ ligand. The energy level localized to the tpy ligand remains only 0.22 eV higher in energy in this scenario, so the lowest-energy absorption band involves MLCT transitions to both tpy and the pyridine rings of $(pbpy\text{-}CO_2H)^-$. We forward the reader elsewhere[32] for a more detailed assignment of the principal transitions for this tridentate series.

The electronic structure for the $[Ru(tpy)(L)Cl]^z$ series differs substantially because of the π^* interaction of the d orbitals with the Cl^- ligand. This repulsion forces the HOMO

(44) Beley, M.; Chodorowski, S.; Collin, J.-P.; Sauvage, J.-P.; Flamigni, L.; Barigelletti, F. *Inorg. Chem.* **1994**, *33*, 2543–2547.
(45) Beley, M.; Collin, J. P.; Sauvage, J. P. *Inorg. Chem.* **1993**, *32*, 4539–4543.
(46) Beley, M.; Collin, J. P.; Louis, R.; Metz, B.; Sauvage, J. P. *J. Am. Chem. Soc.* **1991**, *113*, 8521–8522.

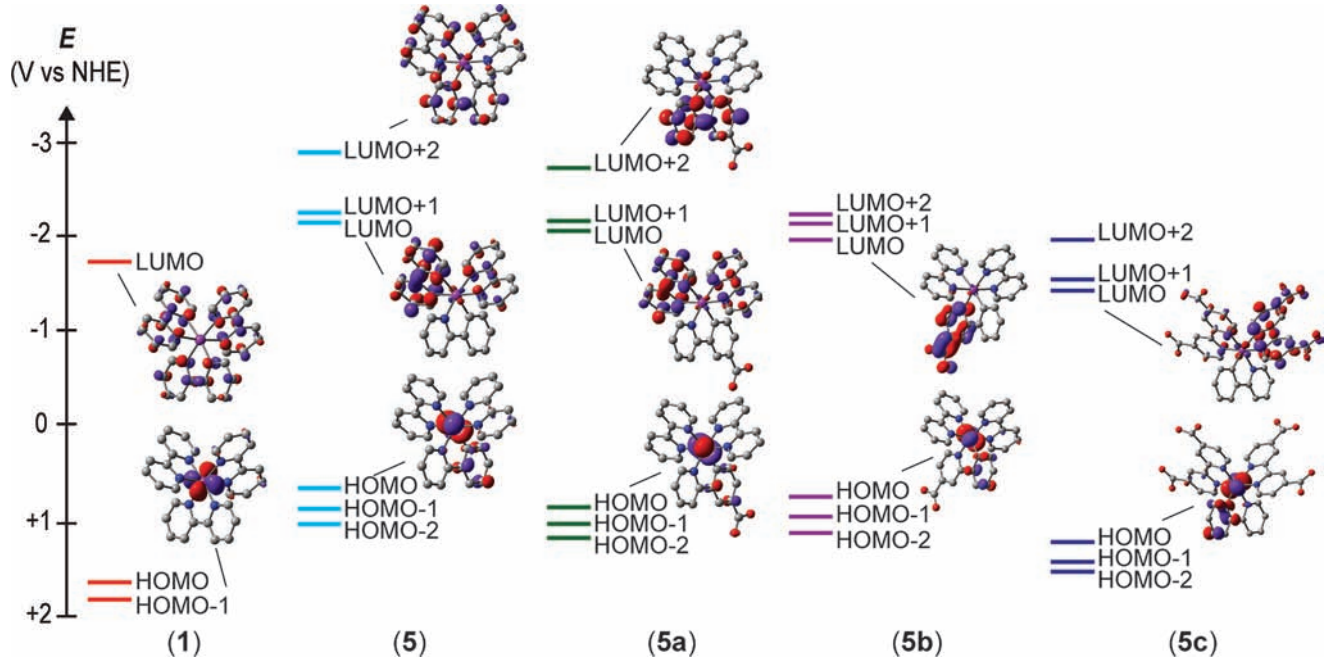

Figure 6. Summary of TD-DFT results for the $[Ru(bpy)_2(C^{\wedge}N)]^z$ series. (Ru = purple; N = blue; O = red; C = gray. H atoms omitted for clarity.).

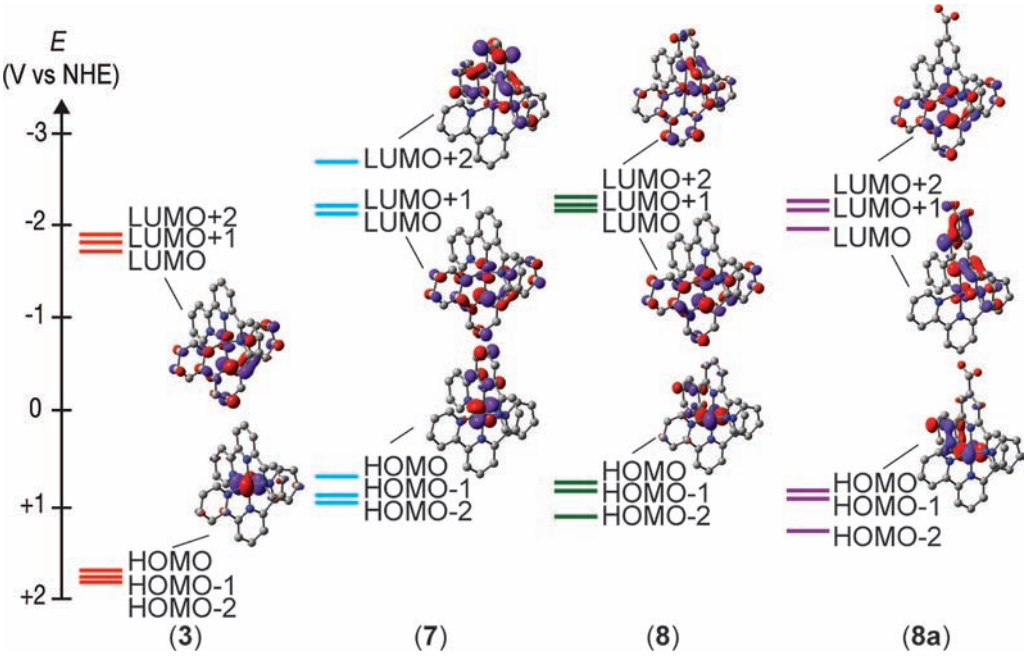

Figure 7. Summary of TD-DFT results for the $[Ru(tpy)(L)]^z$ series. (Ru = purple; N = blue; O = red; C = gray. H atoms omitted for clarity.).

(d_{xy}) and HOMO−1 (d_{yz}) levels higher in energy leaving the d_{xz} orbital as the HOMO−2 in **4**; the low-lying unoccupied orbitals are delocalized over the tpy and bpy ligands (Figure 8). The broad absorption band is due to broad MLCT transitions to both the tpy and bpy ligands, with the shoulder observed at lower energies arising primarily from a Ru→tpy transition. The stable cyclometalated products **9** and **10** exist with the Ru−C_{aryl} bond *trans* to the halide, which drives the metal-halide π^* orbitals to even higher energies. The bonding scheme of the $C^{\wedge}N$ analogues renders the principal axis parallel to the Ru−C_{aryl} bond; thus, the d orbitals are reordered such that the d_{yz} and d_{xz} orbitals comprise the HOMO and HOMO−1 levels, respectively. The d_{xy} orbital is found at HOMO−2 because of the absence of electron repulsion with the filled p orbital of the Cl^- ligand. The LUMO and LUMO+1 levels are localized on the tpy ligand, with the cyclometalating ligand contributing to the LUMO+2 level (which lie ca. 0.50 and 0.35 eV higher in energy than the LUMO for **9** and **10**, respectively). Transitions from the metal orbitals to the tpy ligand and the pyridine ring of ppy^- are responsible for the broad low-energy MLCT bands, while the bands centered at ~400 nm involve charge-transfer to orbitals spanning the entire ppy^- ligand. The minor difference in spectral features between **9** and **10** is due primarily to a slight stabilization of the HOMO for **10**.

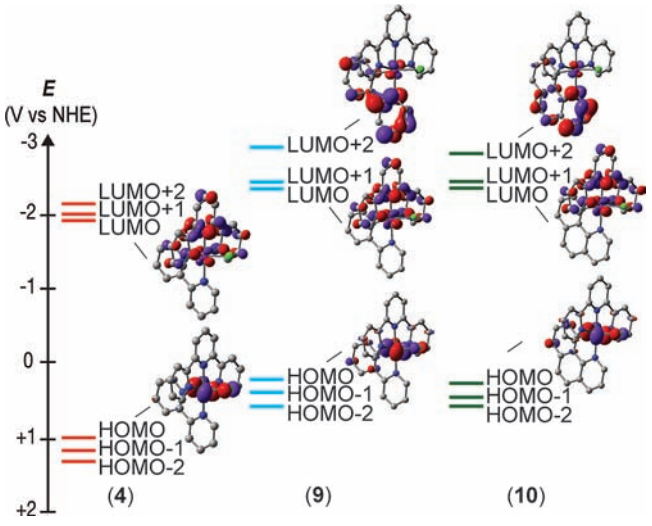

Figure 8. Summary of TD-DFT results for the $[Ru(tpy)(L)(Cl)]^z$ series. (Ru = purple; Cl = green; N = blue; O = red; C = gray. H atoms omitted for clarity.).

Discussion

The complexes in this study were selected to systematically elucidate how the electronic and photophysical properties of pseudooctahedral Ru(II) polypyridyl complexes are disrupted when a single dative Ru−N bond is replaced with an organometallic Ru−C σ-bond. Ru-polypyridyl complexes **1**−**4** were prepared to serve as benchmark compounds to assess the effect of cyclometalation within the series **5**−**10** in both bidentate and tridentate environments (Figure 2). Our overarching goal is to determine whether the electrochemical and photophysical properties of these complexes are appropriate for sensitizing semiconducting materials (e.g., TiO_2) in the context of solar energy conversion schemes (e.g., DSSC). The syntheses of many of the complexes under investigation have been documented previously,[16,17,36−40] but a comprehensive database detailing the properties relevant to sensitization is, in large part, lacking.[32] Furthermore, some of the electrochemical data that has been reported is difficult to corroborate because of inconsistent and incorrect adjustments to the reference electrode.[41] This contribution offers a library of compounds that have all been studied under the same conditions where possible (e.g., solvent, reference electrode) to provide a direct comparison of these properties.

Although there is a wealth of cyclometalated complexes involving late transition metals such as Ir and Pd,[47−52] analogous Ru complexes are less pervasive in the literature.[52] The preparations of cyclometalated Ru complexes are not as rudimentary as those of related complexes **1**−**4**, but relatively facile reaction conditions can drive the requisite C_{aryl}−H activation step to produce reasonable yields of the target complexes. Optimization of the reaction conditions is needed to suppress ligand rearrangement and the formation of homoleptic compounds; thus, isolation of the target compounds often requires purification by column chromatography. We have verified that sufficient electron density at the metal center is needed to drive the C_{aryl}−H activation step: treatment of $RuCl_3$ with any of the cyclometalating ligands employed in this study did not yield a cyclometalated product. We note that other Ru precursors (e.g., $[Ru_2(C_6H_6)_2Cl_4]$[35]) and/or ligand activation steps (e.g., transmetalation with $Hg(L)Cl$[15]) can be utilized to drive the cyclometalation reactions.[52]

Although the incorporation of a single Ru−C_{aryl} bond compromises the molecular symmetry of **1**−**4** to render relatively complicated ^{1}H NMR spectra, the proton adjacent to the organometallic bond provides a convenient handle for monitoring the cyclometalation procedure. With the exception of **7**, this proton is shifted significantly upfield, as are the protons that are *meta* and *para* to the Ru−C_{aryl} bond. In the case of **7**, which is devoid of a proton *ortho* to the Ru−C_{aryl} bond, the *para* proton in the central ring is shifted upfield by about 1.0 ppm to confirm a cyclometalated product. The shielding of the proton adjacent to the organometallic bond by the π system of the central ring of the neighboring tpy ligand was used to determine that of the two possible isomeric forms for **9** and **10**, only the isomer with the Ru−C_{aryl} bond *trans* to the Ru−Cl bond is isolated. Considering that this arrangement forces a π-donating Cl^- ligand opposite a strong σ-donor,[42] we postulate that the resultant isomer is dictated by the electronic demands involving the C−H activation step.

A description of the photophysical properties of these complexes requires an appreciation of the frontier molecular orbitals of the bidentate (e.g., bpy, ppy^-) and tridentate (e.g., tpy, $pbpy^-$, and dpb^-) ligands (Figure 9).[14] The HOMO of bpy, for instance, is predisposed to a σ-bonding interaction to the metal with electron density equally distributed over both N atoms, while the LUMO involves the π^* system of both pyridine rings. In contrast, there is an asymmetric distribution of electron density in the HOMO of ppy^- (localized to the phenyl ring) and LUMO (localized to the π^* system of the pyridine ring). Thus, ppy^- serves as a strong σ-donor through the anionic aryl ring, but the added electron density at the metal is alleviated to an extent by π-backbonding to the pyridyl ring. This also holds true for the $pbpy^-$ and dpb^- ligands; however, symmetry considerations factor into which d orbital interacts with the C_{aryl} atom.

The electrochemical and spectroscopic properties of polypyridyl compounds **1**−**4** have been extensively documented:[6,43] the oxidation wave is assigned to a metal-centered process, while the first reduction wave involves the ligand. Upon cyclometalation, there is an increase in electron density at the metal center to render a HOMO that lies higher in energy, which, in turn, raises the energy of the LUMO because of enhanced π-backbonding to the pyridyl rings, albeit to a lesser degree. These two effects are verified by the electrochemical behavior, which shows respective shifts of the reversible first oxidation and reduction waves of about −0.7 and −0.3 V. TD-DFT studies indicate that the electron density of the metal-based HOMO is delocalized over the cyclometalating ligand; however, the reversible oxidation wave suggests a predominantly Ru-based process. Because the energy of the LUMO for each cyclometalating ligand is

(47) Dijkstra, H. P.; Steenwinkel, P.; Grove, D. M.; Lutz, M.; Spek, A. L.; Van Koten, G. *Angew. Chem., Int. Ed.* **1999**, *38*, 2186–2188.
(48) Fu, Y.; Li, Z.; Liang, S.; Guo, Q.-X.; Liu, L. *Organometallics* **2008**, *27*, 3736–3742.
(49) Hirano, Y.; Saiki, Y.; Taji, H.; Matsukawa, S.; Yamamoto, Y. *Heterocycles* **2008**, *76*, 1585–1592.
(50) Zhang, J.; Khaskin, E.; Anderson, N. P.; Zavalij, P. Y.; Vedernikov, A. N. *Chem. Commun.* **2008**, 3625–3627.
(51) Tamayo, A. B.; Alleyne, B. D.; Djurovich, P. I.; Lamansky, S.; Tsyba, I.; Ho, N. N.; Bau, R.; Thompson, M. E. *J. Am. Chem. Soc.* **2003**, *125*, 7377–7387.
(52) Bruce, M. I. *Angew. Chem.* **1977**, *89*, 75–89.

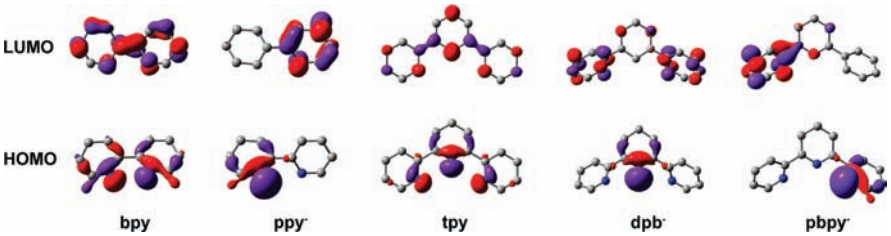

Figure 9. Frontier molecular orbitals of selected polypyridyl and cyclometalating ligands. (Note that the cyclometalating ligands are deprotonated forms of Hppy, Hdpb, and Hpbpy.).

inherently higher than that of the neutral bpy or tpy ligands, the first reduction process is localized on the polypyridyl ligands. This situation can change, however, when an electron-withdrawing substituent (e.g., $-CO_2H$) is attached to the pyridine ring of a cyclometalating ligand (e.g., **5b** and **8a**). This feature underscores the subtle differences in energy levels of the cyclometalating ligands relative to the polypyridyl ligands.

It is well-known that the thermodynamic redox potentials of **1**−**4** correlate reasonably well to their respective absorption profiles; thus, the lowest-energy excitation process is predominantly MLCT in character. The same conclusions are drawn when assessing the properties of the cyclometalated analogues, even with the enhanced ligand character in the HOMO. In all cases, the unoccupied metal-based orbitals reside significantly higher in energy relative to the polypyridyl analogues; thus, transitions within the d-manifold are not observed in the visible portion of the electromagnetic spectrum. In most cases, the lowest-energy electronic transitions are associated with an excited state involving the polypyridyl ligand, with higher energy bands in the visible region corresponding to excited states involving the cyclometalated ligands. This ordering of orbitals is highlighted by comparing **1** to **5**, where the replacement of one bpy ligand with ppy^- in the $[Ru(bpy)_2(L)]^z$ series leads to numerous transitions that are a result of not only a loss of degeneracy of the highest occupied metal orbitals, but also because of a low-lying unoccupied π^* manifold involving both bpy and ppy^-.

These data collectively show that the absorption of light does, in large part, induce a MLCT process reminiscent of Ru-polypyridyl complexes, particularly those that are used as dyes in the DSSC (e.g., **N3**).[8] For these complexes to be viable within the DSSC, the excited- and ground-state oxidation potentials must also be appropriately matched to the TiO_2 conducting band (E_{cb}) and the redox couple of the electrolyte (e.g., I^-/I_3^-), respectively. For the most part, the thermodynamic potentials of the cyclometalated compounds appear to be well-suited for the DSSC. As shown in Figure 10, the π^* orbitals of the ligands are shifted to higher energy, and therefore remain poised for electron-injection into the E_{cb} of TiO_2, while the ground-state oxidation potentials for **5**−**8** are properly positioned to interact with the electrolyte. The ground-state oxidation potentials of **9** and **10** are too high in energy, and can therefore be ruled out for study in the DSSC where I^-/I_3^- is used as the electrolyte, unless electron withdrawing substituents are installed on the molecule.

The position of the anchoring group about the ring system of the polypyridyl and/or cyclometalating ligands must also be taken into careful consideration for chromophore design. For instance, optimal sensitization of an n-type semiconductor requires that the $-CO_2H$ substituent be

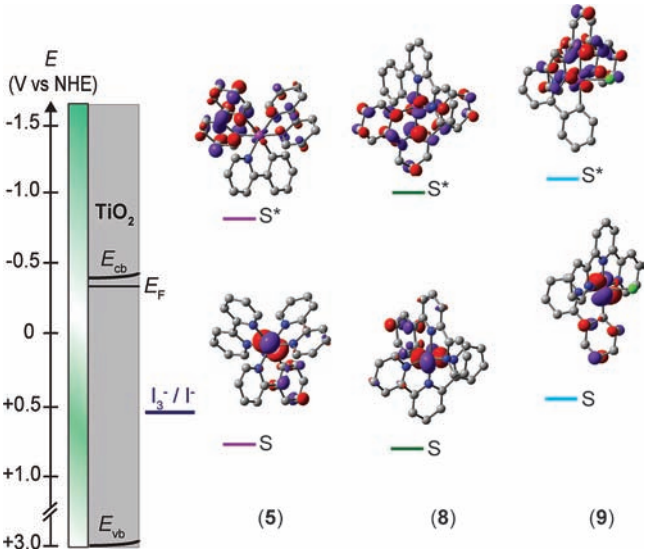

Figure 10. Energy level diagram depicting the HOMO and LUMO of **5**, **8**, and **9** relative to the redox couple of I^-/I_3^- and the E_{CB} of TiO_2. (S and S* are defined by experimental $E_{1/2,ox1}$ and $E(S^*/S^+)$ values, respectively.)

positioned on the dye where there is sufficient electron density in the excited state to mediate electron transfer. For the type of dyes presented in this work, the anchoring group should therefore be positioned on the polypyridyl ligands − *not* on the cyclometalated ligand − to optimize electron injection into TiO_2 *and* to enhance the ε value.[53] This point is fortuitous within the bidentate series because the dcbpy ligands of **5c** also provide the greatest bathochromic shift relative to **5**. Moreover, this motif is effectively the same as **N3**, except that the two monodentate NCS^- ligands have been replaced by a $C^\wedge N$ ligand. Considering that the absorption profile of **5c** mirrors the broad envelope of **N3**, yet is even more red-shifted, complexes of this type have the potential to be very efficient sensitizers (see Supporting Information for a comparison of absorption spectra). In stark contrast to the NCS^- groups found in conventional dyes, however, the cyclometalating ligands provide a platform for further tuning the ground-state oxidation potentials. For instance, if it turns out that dye regeneration is inefficient, electron-withdrawing groups on the phenyl ring of the ppy^- ligand would lower the energy of the HOMO to provide a larger driving force for dye regeneration by I^-. Indeed, this concept was proven successful in the form of $[Ru(dcbpy)_2(ppy\text{-}F_2)]^+$.[30] We therefore contend that these $[Ru(bpy)_2(C^\wedge N)]^+$ and $[Ru(tpy)(C^\wedge N^\wedge N)]^+$ (or $[Ru(tpy)(N^\wedge C^\wedge N)]^+$) series of

(53) Koivisto, B. D.; Robson, K .C. D.; Berlinguette, C. P. *Inorg. Chem.* **2009**, DOI: 10.1021/ic9007137.

compounds represent a promising platform of chromophore design in the context of the DSSC.

Conclusions

Electrochemical and spectroscopic methods were used to show that the strong σ-donating ability of cyclometalating ligands push the ground-state oxidation potentials of Ru(II) complexes to significantly higher energies. The π^* system of the cyclometalating ligands reside only slightly higher in energy than those of the polypyridyl ligands, a feature that yields multiple, intense absorption bands in the visible region of the electromagnetic spectrum at higher energies than their polypyridyl congeners. This feature offers much promise for light-harvesting applications; indeed, we have established that many of these complexes exhibit thermodynamic potentials that are favorable for the DSSC setting. Studies are currently underway to test these complexes in the DSSC, and to gain a better understanding of their excited-state properties. We are also seeking ways to increase the molar extinction coefficients of these complexes to further improve their light-harvesting ability.

Acknowledgment. The authors thank Prof. Ray Turner and Prof. Warren Piers for access to instrumentation, and Dr. Bryan Koivisto for synthetic assistance. This work was financially supported by the Canadian Natural Science and Engineering Research Council (NSERC), Canada Research Chairs, Canada Foundation for Innovation, Alberta Ingenuity, Canada School for Sustainable Energy, and The Institute for Sustainable Energy, Environment & Economy. P.G.B. acknowledges NSERC and Alberta Ingenuity for financial support.

Supporting Information Available: Calculated UV−vis spectra for all compounds, a comparison of the absorption profiles of select compounds with the **N3** dye, and a summary of the TD-DFT results. This material is available free of charge via the Internet at http://pubs.acs.org.